Non-across-wind galloping of a square-section cylinder

Cung H. Nguyen [a], John H. G. Macdonald [b], Stefano Cammelli [c]

[a]*Industrial University of Ho Chi Minh City, Ho Chi Minh City, Vietnam*
[b]*University of Bristol, Bristol, United Kingdom*
[c]*WSP UK Ltd., London, United Kingdom*

ABSTRACT

This paper presents new insights on the galloping instability phenomenon of square-section prisms. The role of the orientation of the structural axes on the galloping response is studied through wind tunnel tests and quasi-steady theory. A new series of dynamic wind tunnel tests on a square section model were conducted to evaluate non-across-wind galloping vibrations, as well as conventional across-wind galloping. The results are then compared with theoretical predictions to evaluate the reliability of quasi-steady theory in assessing the galloping phenomenon. It is found that for a given angle of attack, the structure has different aeroelastic behaviour for different orientations of the principal axis. At an angle of attack close to the critical angle of attack of square prisms, the quasi-steady theory well predicts the critical wind velocity for the onset of non-across-wind galloping but it is not successful for the case of across-wind galloping.

Keywords: Non-across-wind, Across-wind, Galloping, Wind tunnel tests, Quasi-steady theory, Square section

1. Introduction

Wind-induced instability of square cylinders is one of the most frequently investigated issue in fluid-structure interaction. Vortex-Induced Vibrations (VIV) and galloping are the two main aeroelastic phenomena of a square prism subjected to wind flow that can lead to dynamic instability and large amplitude vibrations of the prism. For transverse galloping, many theoretical and experimental studies have been developed to predict the occurrence of onset galloping and post-critical oscillation amplitudes. However, good agreement between theories and experiments has not been always found, making the topic still of interest for investigation [1, 2].

The first studies of transverse galloping of square prisms date back to the 1960's with wind

tunnel experiments by Scruton [3] and Parkinson and Brook [4]. Later, pioneering work by Parkinson and Smith [5] showed good agreement between their proposed theory and wind tunnel tests for predicting the onset and post-critical across-wind galloping responses of a square prism. They were the first to show the existence of a hysteresis phenomenon for galloping. Another key study on transverse galloping was by Novak [6], who derived an analytical solution of the oscillation amplitudes in the hysteresis zone, developing the concept of a “universal curve”. According to this analysis, galloping amplitudes of a prism of a given cross-sectional shape collapse onto this curve, regardless the values of structural parameters such as sectional size, mass, stiffness and damping. Novak’s theory has been confirmed through wind tunnel tests on different sectional shape prims, such as L-sections [7], rectangular sections [6, 8, 9]. Further wind tunnel experimental investigations have, however, showed that the Novak's theory does not always work [1, 10]. Other studies on transverse galloping have been intensively reviewed by Blevins [11] and [12], and critically discussed by Piccardo et al. [13].

It is worth noting that in the investigations mentioned above on transverse galloping of square prims, particularly in wind tunnel experiments on one degree-of-freedom (1DOF), the angle of attack was zero, i.e. the wind was along a line of symmetry of the body, and the body was only free to vibrate in the across-wind direction. However, this may not necessarily represent the case in practice as in general the structural response may be in any direction, depending on the relationship between the wind direction, orientation of the cross sectional shape and, most importantly, the orientation of the principal structural axes [14, 15]. This means that, if a principal structural axis is not perpendicular to the wind, galloping may still occur, but in a non-across-wind direction. To the authors’ knowledge, although the importance of further wind tunnel investigations of the structural aeroelastic behaviour for angles of attack different from zero was emphasised [12], there were only a few aeroelastic tests on square prism for various angles of attack [16–18]. Furthermore, the issue of non-across-wind vibrations has never previously been tested in wind tunnels, except for circular and elliptical cable models, most of which were for 2DOF vibrations [19–21], and a few of which were 1DOF vibrations [22, 23]These investigations, however, mainly focused on three-dimensional effects involving skew of the cables relative to the wind.

Starting from these observations, this paper presents new wind tunnel tests to investigate the aerodynamic loads and galloping responses of a square-section prism to provide further insight on the phenomenon. In this study, the role of the orientation of the structural axes of the body is addressed through a series of new campaign of wind tunnel tests carried out for cases of across-

wind and non-across-wind vibrations and at angles of attack different from zero.

The paper is structured as follows: Section 2 provides a brief formulation for galloping occurrence using quasi-steady hypothesis; Section 3 presents the details of the wind tunnel testing set-up and of the testing campaign (the tests included static tests to estimate the aerodynamic coefficients of the cylinder in order to determine the critical conditions for the onset of galloping through quasi-steady theory and dynamic wind tunnel tests to measure directly the aeroelastic responses in across-wind and non-across-wind flows); Section 4 analyses and discusses the results obtained from the wind tunnel tests; and, finally, critical comments are provided in Section 5.

2. Quasi-steady formulation for the occurrence of galloping

Let us consider a prismatic cylinder subjected to wind flow with mean velocity U, oscillating in direction y with velocity $\dot{y}$, making a relative angle of attack α^* of a relative direction of the wind with velocity U^* at an instant time (Fig. 1). The instantaneous drag and lift forces are defined with respect to the relative velocity U^* as shown in Fig. 1. Axes x and y are the principal axes. It is assumed here that motion in the x direction is restricted. Axes x_0 and y_0 are the reference axes on the body used to define the angles of attack, α , as shown in the figure.

At a wind direction with an angle of attack α, the cylinder can oscillate in an across-wind (Fig. 1a) or non-across-wind (Fig. 1b) direction depending on the angle, γ, between the wind, U, and the principal axis y. The angle between the reference axis y_0 and the principal axis y is $\beta=90+\alpha-\gamma$.

Normally, the condition for the onset of galloping, i.e. Glauert-Den Hartog criterion is formulated by considering across-wind oscillation, i.e. $\gamma=90^o$ (Fig. 1a), and $\alpha=0$ (e.g. [1, 5, 14, 24, 25]. Similarly, conventional galloping wind tunnel tests address this case. The definition of the angles in Fig. 1 is more general, where the wind direction and the orientations of structural axes and reference axes are arbitrary.

Previous works on across-wind galloping analysis adopting quasi-steady theory are referred to the review book by Paidoussis et al. [12]. Based on that, the following sub-section re-formulates the critical condition for the onset of across-wind galloping through the quasi-steady theory. The quasi-steady formulation is then extended for the non-across-wind case, with a general angle γ (Fig. 1b), in Section 2.2.

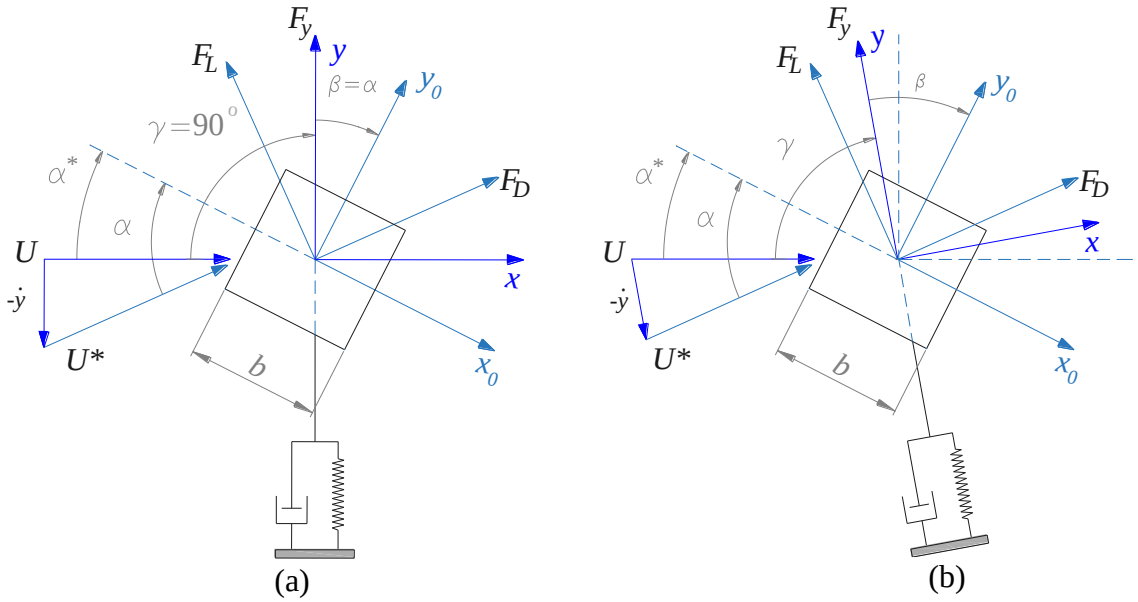

Fig. 1 Cross-section subjected to mean wind velocity, U, indicating angles γ and α between the wind velocity and principle axis (y) and body reference axis (x_0) – (a) across-wind oscillation, i.e. γ=90; (b) non-across-wind oscillation

2.1. Across-wind galloping

The equation of motion in the y-direction is given by

$$\ddot{y}_r + 2\xi\dot{y}_r + y_r = \frac{n}{4\pi^2}U_r^2 C_{F_y} \tag{1}$$

where y_r, U_r, ξ, C_{F_y} and n are the reduced displacement, reduced wind velocity, damping ratio, coefficient of the aerodynamic force F_y and mass ratio, respectively. The dot denotes the derivative with respect to reduced time. The reduced quantities and the mass ratio are given by

$$U_r = \frac{U}{fb};\ y_r = \frac{y}{b}\ ;\ n = \frac{\rho b^2}{2m} \tag{2}$$

where U, b, f, m and ρ are the wind velocity, characteristic width of the cross-section, natural frequency, mass per unit length, density of air , respectively.

The aerodynamic force coefficient C_{F_y} can be evaluated through the drag coefficient C_D and lift coefficient C_L at the instantaneous angle α

$$C_{F_y} = C_D \sin\left(\alpha^* - \alpha\right) + C_L \cos\left(\alpha^* - \alpha\right) \tag{3}$$

For α=0°, the coefficient C_{F_y} given by Eq. (3) is equivalent to that provided by other studies e.g. [12, 14, 26]. Adopting the quasi-steady theory, C_{F_y} can be determined through static wind tunnel tests as shown in Section 3.

Through a Taylor series expansion and ignoring the non-linear terms, the coefficient C_{F_y} can be also expressed as follows

$$C_{F_y} = C_{F_y}\Big|_{\alpha^*=\alpha} + \left.\frac{\partial C_{F_y}}{\partial \alpha^*}\right|_{\alpha^*=\alpha} \left(\alpha^* - \alpha\right) \tag{4}$$

For a small $\left(\alpha^* - \alpha\right)$ which results in $\alpha^* - \alpha \simeq -\dot{y}/U = -2\pi \dot{y}_r / U_r$, substituting Eq. (3) into Eq. (4) and then Eq. (4) into Eq. (1), ignoring the equilibrium component given by the first term of the right hand side of Eq. (4), yields

$$\ddot{y}_r + 2\left(\xi + \xi_a\right)\dot{y}_r + y_r = 0 \tag{5}$$

where ξ_a is the aerodynamic damping ratio, defined as

$$\xi_a = \frac{\rho b U \left(C_D + C_L'\right)}{8\pi f m} \tag{6}$$

where C'_L is the derivative of the lift coefficient with respect to the angle of attack.

Galloping occurs when the total damping ($\xi + \xi_a$) in Eq. (5) is negative. As the structural damping ξ is always positive, a necessary condition for the occurrence of galloping is that the aerodynamic damping coefficient ξ_a is negative [27, 28], which occurs when

$$S_a < 0 \tag{7}$$

where S_a is the galloping factor, given by

$$S_a = C_D + C_L' \tag{8}$$

The reduced critical velocity for the onset of galloping can be obtained by setting the total damping zero, yielding

$$U_{cr,r} = -\frac{2Sc}{S_a} \tag{9}$$

where *Sc* is the Scruton number, defined as

$$Sc = \frac{4\pi\xi m}{\rho b^2} \tag{10}$$

To investigate galloping response in the post-critical condition, Parkinson and Smith [5] solved Eq. (1), considering the nonlinear aerodynamic effects, to evaluate the oscillation amplitudes of a prism subjected to uniform wind. In this study, the aerodynamic force coefficient C_{F_y} was approximated as a polynomial function to find the hysteresis amplitude curve. The galloping hysteresis phenomenon was shown to exhibit good agreement between the theory and wind tunnel tests. Extending the pioneering work of Parkinson and Smith, Novak [6] derived the analytical solution for the oscillation amplitude in the hysteresis zone. Moreover, he showed that all the galloping amplitudes of a given prism collapse onto a single curve, named the "universal curve", for different values of the parameters including size, mass ratio, stiffness and damping. This curve is found through scaling the system (U_r, y_r) with a factor $\lambda_N = n/2\xi$, referred to as Novak's coefficient.

2.2. Non-across-wind galloping

Generally, the wind has an arbitrary direction and not necessarily normal to the structural principal axis. Then from Fig. 1b, the coefficient C_{F_y} given in Eq. (3) can now be generalised in the following form

$$C_{F_y} = C_D \sin\left(\alpha^* - \beta\right) + C_L \cos\left(\alpha^* - \beta\right) \tag{11}$$

The necessary condition and critical velocity for the occurrence of galloping are as expressed in Eq. (7) and Eq. (9), respectively, but the galloping factor S_a is now replaced by [14, 29]

$$S_{ay} = C_D\left(1+\cos^2\gamma\right)-\left(C'_D + C_L\right)\sin\gamma\cos\gamma + C'_L\sin^2\gamma \qquad (12)$$

When $\beta=\alpha$, equivalent to $\gamma = 90^o$, Eq. (11) simplifies to the same as Eq. (3) while Eq. (12) simplifies to the same as Eq. (8), obtaining the classic across-wind galloping factor.

For a given configuration of a cross section and a given angle of attack, the difference between Eq. (8) and Eq. (12) evidently shows the incorrect evaluation the onset of the occurrence of the galloping when using the Glauert-Den Dartog criterion. Meanwhile, the difference between Eq. (3) and (11) shows the different behaviour between the across-wind and non-across-wind galloping responses, indicating the Novak's solution valid only for the case of across-wind galloping.

3. Wind tunnel experimental investigations

To assess the accuracy and reliability of quasi-steady theory in predicting the galloping instability for the case of non-across-wind flow, static and dynamic tests on a 140mm x140mm square section model were conducted in the Teddington aeronautical wind tunnel which, at the time of the testing campaign, was managed and operated by BMT Fluid Mechanics Ltd. The tunnel has an octagonal cross section test section, which is 2.74 m wide and 2.14 m high. Without any turbulent generators, the wind tunnel produces wind flows with turbulence intensity less than 1%. It can provide wind speeds varying from 0.2 m/s to 65 m/s. Static tests aimed to determine the aerodynamic coefficients in smooth flow Dynamic tests aimed to measure the oscillation amplitudes, allowing comparison of the results with the theoretical predictions. Only smooth flow was considered during the tests, i.e. without using turbulent generator. The inflow conditions can affect the aerodynamics and hence the dynamic responses [30, 31]. As detailed in Section 3.2, the experimental setup was arranged to capture the vibrations for both across-wind and non-across-wind directions.

3.1. Static tests

In the static tests, a prismatic cylinder with a square section was attached to stiff machined-aluminium end cubes, which allowed the model to be fixed to force balances at both ends (Fig. 2a). The force balance measurements were used to determine the aerodynamic drag and lift coefficients, defined as

$$C_D = \frac{\mathrm{E}\left[F_D\right]}{0.5\rho bLU^2} \;\; ; \;\; C_L = \frac{\mathrm{E}\left[F_L\right]}{0.5\rho bLU^2} \qquad (13)$$

where E[•] is the statistical average operator, implemented as a time average over 4 minutes adopting the hypothesis of ergodic behaviour; U is the undisturbed mean wind velocity; L is the length of the model (L= 2730 mm); b is the width of the cross section (b=140 mm); F_D and F_L are, respectively, the measured drag and lift forces, and their signs are conventionally defined as in Fig 2b.

The coefficient C_{F_y} associated with y-axis can be evaluated through the static coefficients C_D and C_L as follows

$$C_{F_y} = C_D \sin(\alpha - \beta) + C_L \cos(\alpha - \beta) \tag{14}$$

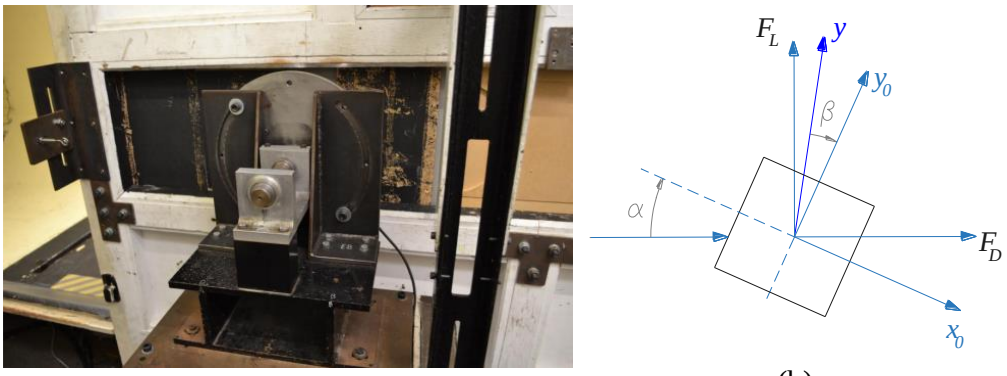

(a) (b)

Fig. 2 (a) Force balance rotating system; (b) Force sign convention

Static tests were conducted for an angle of attack α varying from -2° to 20° with a step of 2° and at two wind speeds: 6.7 m/s and 8.4 m/s. To check the influence of Reynolds number, at α =12° tests were carried out at four wind speeds: 5.9 m/s, 6.7 m/s, 7.7 m/s, and 8.4 m/s, corresponding to Reynolds numbers (based on the width of the section) of 54.4×10^3, 62.7×10^3, 70.8×10^3, 78.9×10^3. The blockage ratio was very low (<2.5%), so no data correction has been adopted with reference to the blockage ratio.

Fig. 3a-b shows the variation of the drag coefficient C_D and lift coefficient C_L with respect to the angle of attack at Reynolds number of 62.7×10^3. No significant influence of Reynolds number was found in the tests. It can be seen that the critical angle of attack for both C_D and C_L, defined as the angle where the coefficient has the largest absolute value, is 14°. The coefficients agree reasonably well with data available in the literature, e.g. [32–34].

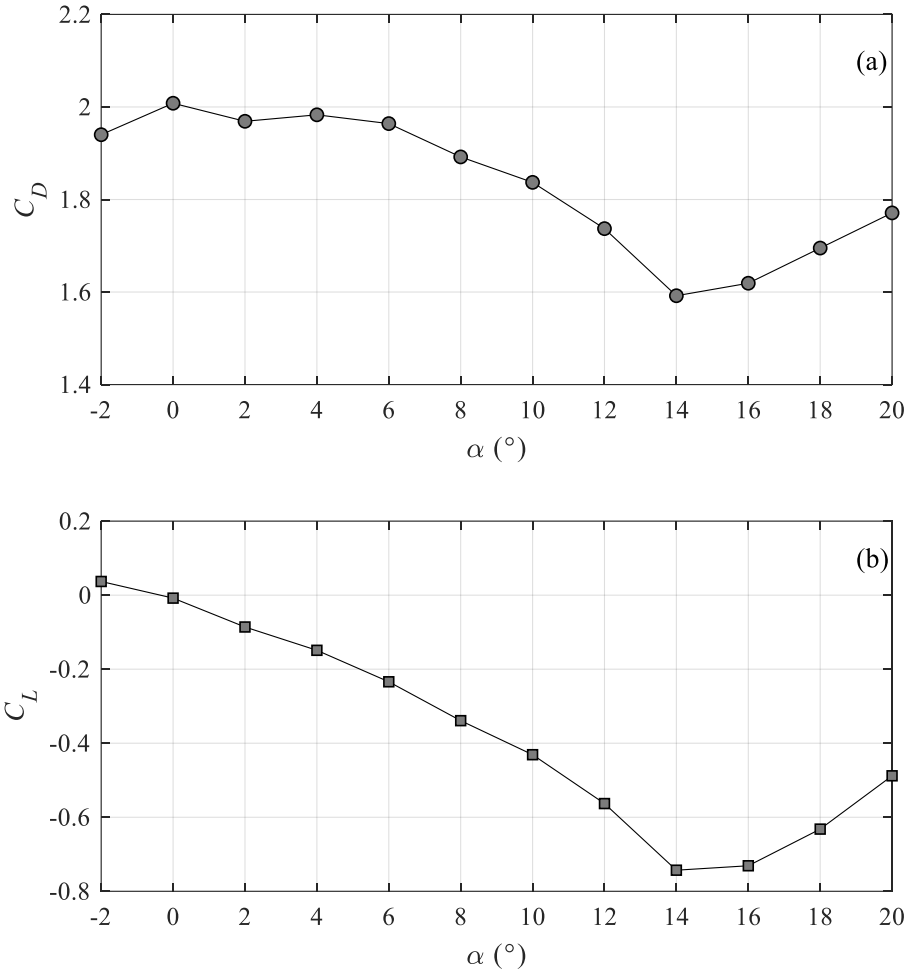

Fig. 3 Variation with respect to the angle of attack of: (a) Drag coefficient; (b) Lift coefficient

From the measured aerodynamic coefficients, Fig. 4 shows the force coefficient C_{F_y} for various angles γ between the wind direction and the *y*-axis. It can be seen that for a given cross section and a given angle of attack, the orientation of the structural axis strongly affects the force coefficient. Previous studies on across-wind galloping have often fitted the force coefficient C_{F_y} as a function of angle of attack using a polynomial function [1, 5, 8] or a spline interpolation [26]. The fitted function has enabled Eq. (1) to be solved to obtain the amplitude of galloping responses in the form of a non-dimensional "universal curve" [8, 26]. In this study, the dependence of the force coefficient on the orientation of the structural axis implies that for each angle γ, the coefficient C_{F_y} has a different fitting function. As a result, for the same angle of attack, the existence and location of the inflection point of C_{F_y} for different cases of γ are different, leading to different galloping universal curves and hysteresis behaviour [35, 36].

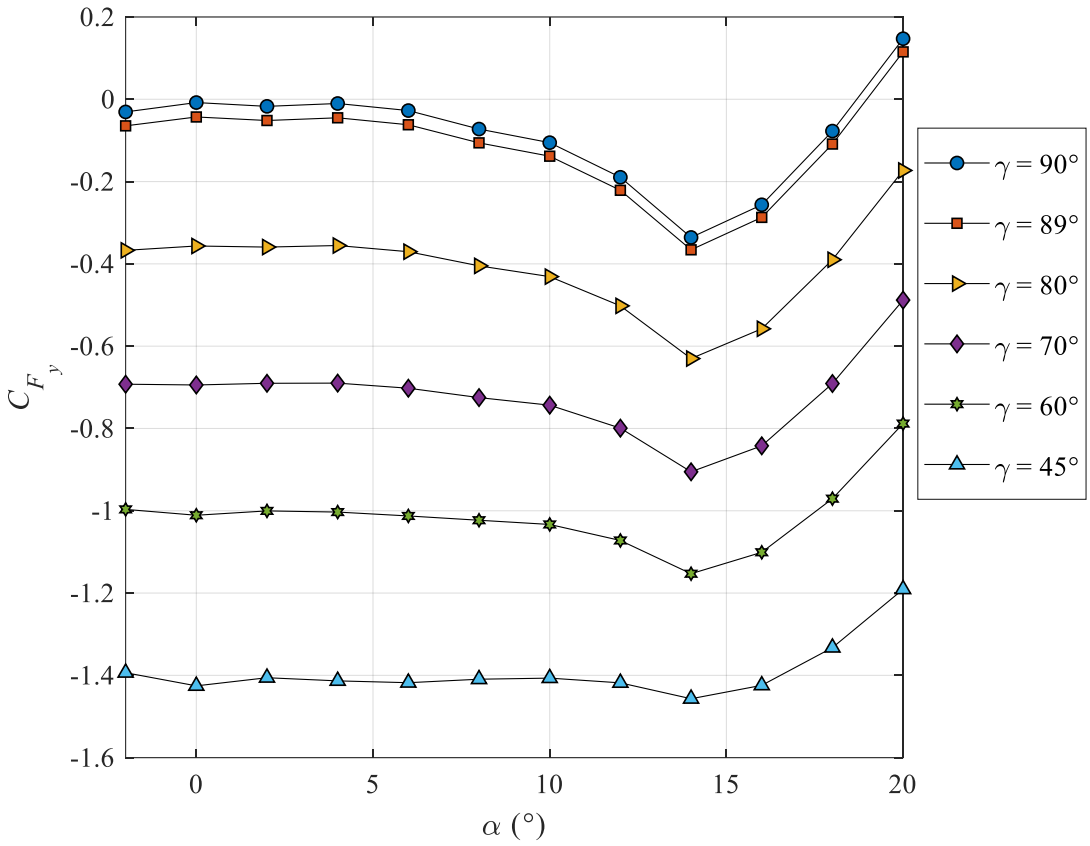

Fig. 4 Force coefficients C_{F_y} for different orientation of the structural axis *y*

To visualise the effect of the orientation of the structural axis on the onset of the galloping, Fig. 5a shows the galloping factor S_a, given by Eq. (12), and Fig. 5b shows reduced critical galloping velocity, given by Eq. (9), for three cases γ=90º, γ=82º and γ=80º. Any reduced critical velocities higher than 50 are excluded from the Fig. 5b. The derivatives of C_D and C_L with respect to angle of attack were determined through a smoothing spline approximation.

It can be observed that the cylinder is prone to gallop at most angles of attack from 4º to 14º, where S_a is negative. Importantly, for a given angle of attack, S_a is more negative for the larger angles γ from 80º to 90º, showing that, among the considered cases, the critical galloping velocity is lower for the across-wind case than for the non-across-wind cases. On the hand, for the angles of attack from 0º to 2º, the occurrence of the onset galloping can be found only for the case of across-wind oscillation, i.e. γ=90º. Therefore, for the angles of attack from 0º to 14º, the structure is more unstable for the principal axis *y* more inclined to the wind.

It can be also seen from Fig. 5a that S_a is sensitive to the angle of attack. Consequently, this

may lead to large differences in the prediction of the critical wind velocity using quasi-steady theory for small changes in angle of attack. Furthermore, the accuracy of the predictions may be affected by uncertainties in measuring the aerodynamic coefficients and the fitting method used for C_D and C_L and hence to evaluate S_a, especially in estimating the gradient C'_L [37].

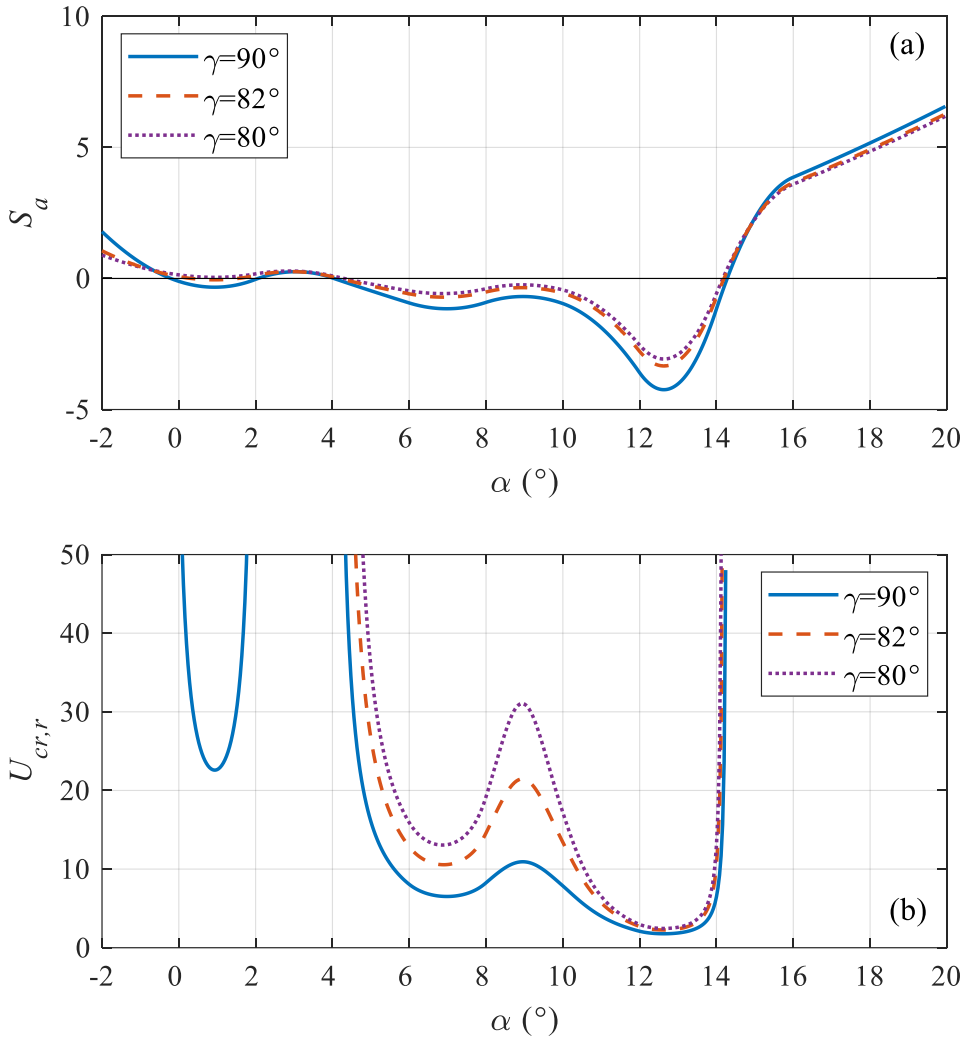

Fig. 5 (a) Galloping factor and (b) reduced critical wind speed for the onset of galloping

3.2. Dynamic tests

To investigate the influence of the orientation of the structural axes on the aeroelastic behaviour of the sectional model and to assess the validity of quasi-steady theory in predicting the critical conditions for galloping occurrence at different orientations, dynamic tests were carried out at an angle of attack of α = 10° for three orientations of principal axes: (1) γ=90°; (2) γ=82° and (3)

γ=80^o. The first case is as in conventional dynamic wind tunnel tests for across-wind galloping. To give further insight for non-across wind galloping, for γ=80^o more tests were conducted for different Scruton numbers by changing the damping ratio.

Fig. 6 shows the setup of the dynamic tests. Each end of the model was mounted on a dynamic rig consisting of a system of springs allowing 1DOF motion in *y* direction. Stiff wires were installed horizontally to restrain the motion in the horizontal direction. To measure the dynamic responses a laser system with Micro Epsilon Opto NCDT lasers was used (Fig. 6c). An electro-magnetic damping system, consisting of copper plates moving through magnetic fields (Fig. 6c), was used to provide additional damping.

Table 1 shows the parameters for the dynamic tests for all five setups used, including the values of the effective model mass per unit length *m* (allowing for additional masses and the mass of the support structure), structural damping ratio ξ, natural frequency *f*, and Scruton number *Sc*. For each setup, the natural frequency, damping ratio and principle axes were estimated through free-decay tests, using frequency transform technique and logarithmic decrement method. The natural frequencies in the two principle axes were well separated, showing the 1DOF motion in the *y* direction.

Table 1. Parameters in dynamic tests

Setup ID	γ	*m* (kg/m)	ξ (%)	*f* (Hz)	*Sc*
1	90°	7.69	0.60	3.27	23.7
2	82°	6.39	0.40	3.54	13.1
3	80°	7.69	0.27	3.26	10.8
4	80°	7.69	0.32	3.26	12.6
5	80°	7.69	0.33	3.26	13.0

Tests were carried out using increasing and decreasing wind speeds with small increments (less than 1 *m/s*), aiming to capture any hysteresis of the response. The steady state oscillation amplitudes, normalised by the width of the section, were identified (y_r). The amplitudes were recorded after steady conditions were obtained for every wind speed change. The duration of each record was 40 seconds. The results are shown and discussed in Section 4.

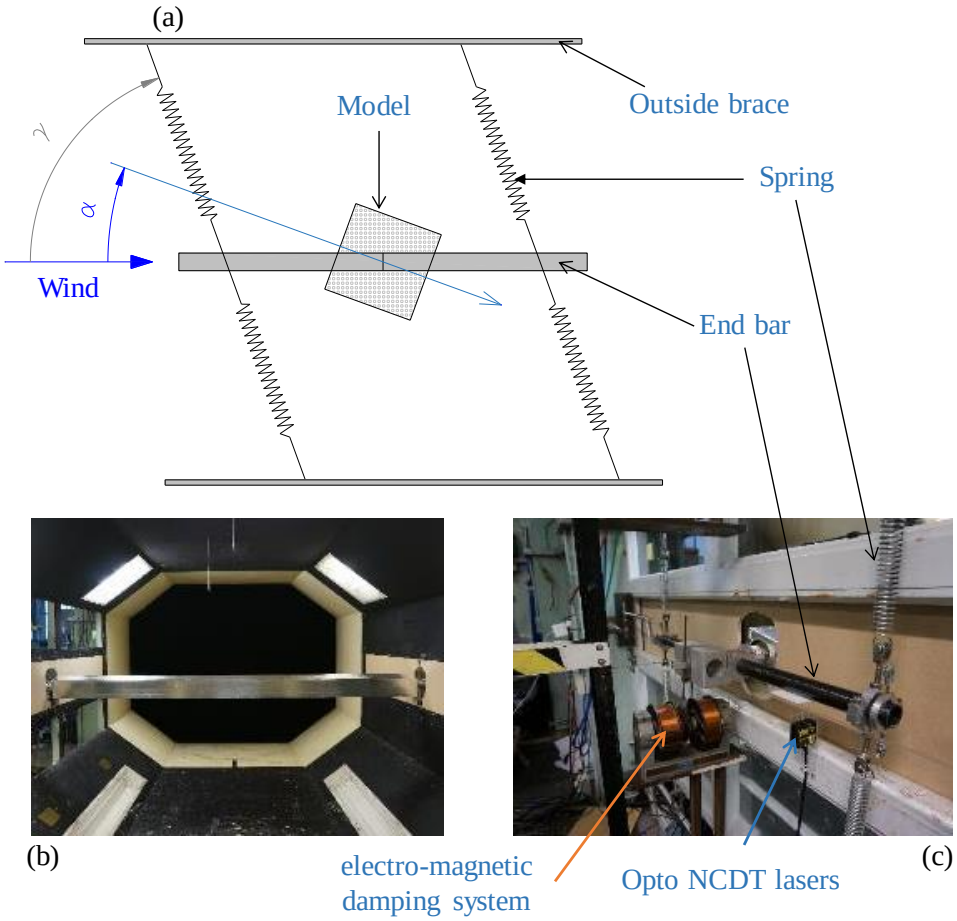

Fig. 6 Dynamic wind tunnel test setup: Schematic of the testing arrangement; (b) Model in the test section; (c) Springs and damping system

4. Across-wind and non-across-wind galloping responses

4.1. Oscillation responses

Fig. 7 shows an example of buffeting (Fig. 7a) and steady-state (Fig. 7b) responses, each over 40 seconds long. At a given wind speed, the displacement response is evaluated as the r.m.s of the 40-second time history response. The evaluation of VIV and galloping responses are based on steady-state responses.

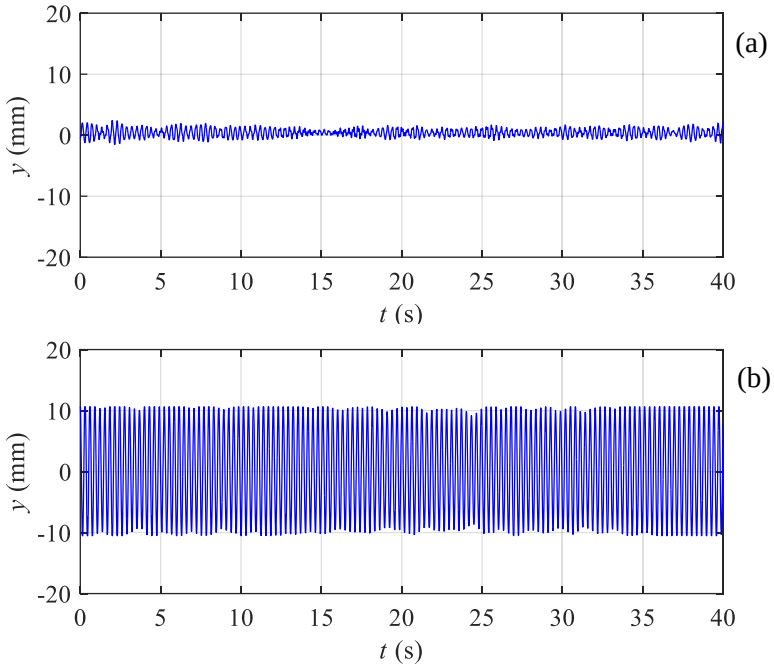

Fig. 7 Example of time history responses: (a) buffeting response; (b) steady-state response

Fig. 8a-e shows the reduced vibration amplitude versus the reduced wind speed for the five setup, all for α=10°. In the tests, large amplitudes due to vortex-induced vibrations (VIV) at lower wind speeds and from galloping at higher wind speeds were detected. Table 2 shows the values of critical velocity for VIV and galloping, in which $U_{V,r}$ and $U_{G,r}$ are respectively the reduced critical velocity for VIV and galloping obtained from the tests while $U_{cr,r}$ is the reduced critical galloping velocity obtained from quasi-steady theory. The reduced velocities are normalised as in Eq. (2). No interaction between VIV and galloping was observed during the tests.

It can be seen from Fig. 8 and Table 2 that the reduced critical velocities for VIV for the five cases are between 7.56 and 8.17. These values are close to the theoretical value $U_{V,r}$=1/St =7.69, where the Strouhal number St=0.13 for a square section [38, 39]. Despite this similarity, for a given angle of attack, the variation of reduced VIV critical wind speeds and of the shape of VIV responses for different Scruton number and orientations of the structural axis highlight the role of these conditions for VIV responses. The issue of the structural axis orientation has never been investigated seriously in the literature.

In four of the five cases (Setups 1, 2, 4 and 5, corresponding to Fig. 8a-b, Fig. 8d-e), the critical velocity for galloping is at least twice as higher as the critical velocity for VIV, i.e. $U_{G,r} \geq$

$U_{V,r.}$ In these cases, galloping and VIV are clearly separated. For the case of Setup 3 where the ratio between the two critical velocities $U_{G,r}/U_{v,r}$ =1.79, the distinction between the two phenomena is not fully clear, although no interaction has been detected. This result agrees with the literature for across-wind vibrations of square section prisms (e.g. [40, 41]). For practical engineering application, Eurocode specifies a ratio 1.5 for the separation of the two phenomena, for the case of wind normal to the direction of motion [42].

To check if VIV and galloping are separated, beside using the ratio $U_{G,r}/U_{v,r,}$ as a criterion, the Scruton number (*Sc*) has been applied in the literature. Scruton [3], who first investigated VIV-galloping interaction of square cylinders across-wind, showed that the two phenomena are distinct when *Sc*>10; otherwise interference between them may appear [12]. Recent research by Freda et al. [1] and Ma et al. [2], also for a square cylinder across-wind, came to similar conclusions. This is also found to be the case in this study for non-across-wind aeroelastic responses. As seen in Fig. 8 and Table 2, the two phenomena are well separated for *Sc* noticeably higher than 12 (Setup 1, 2, 4 and 5) but are not so well separated for *Sc* is close to 10 (Setup 3).

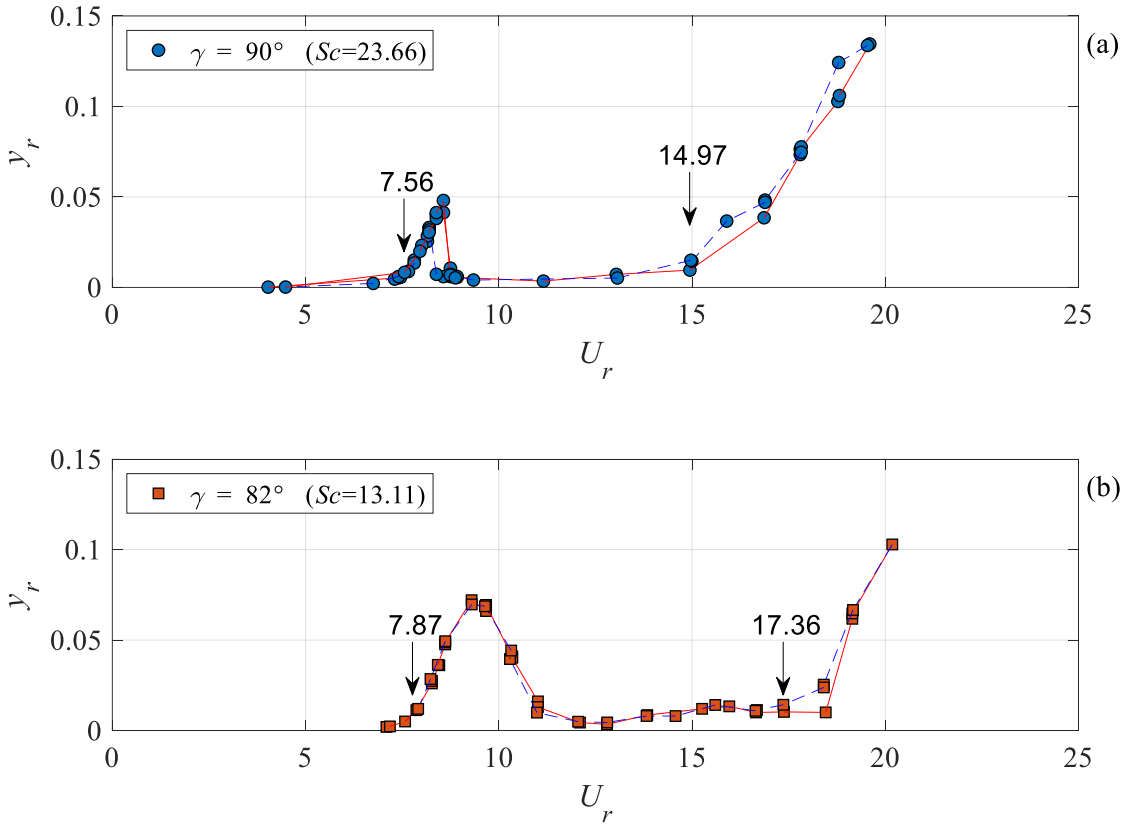

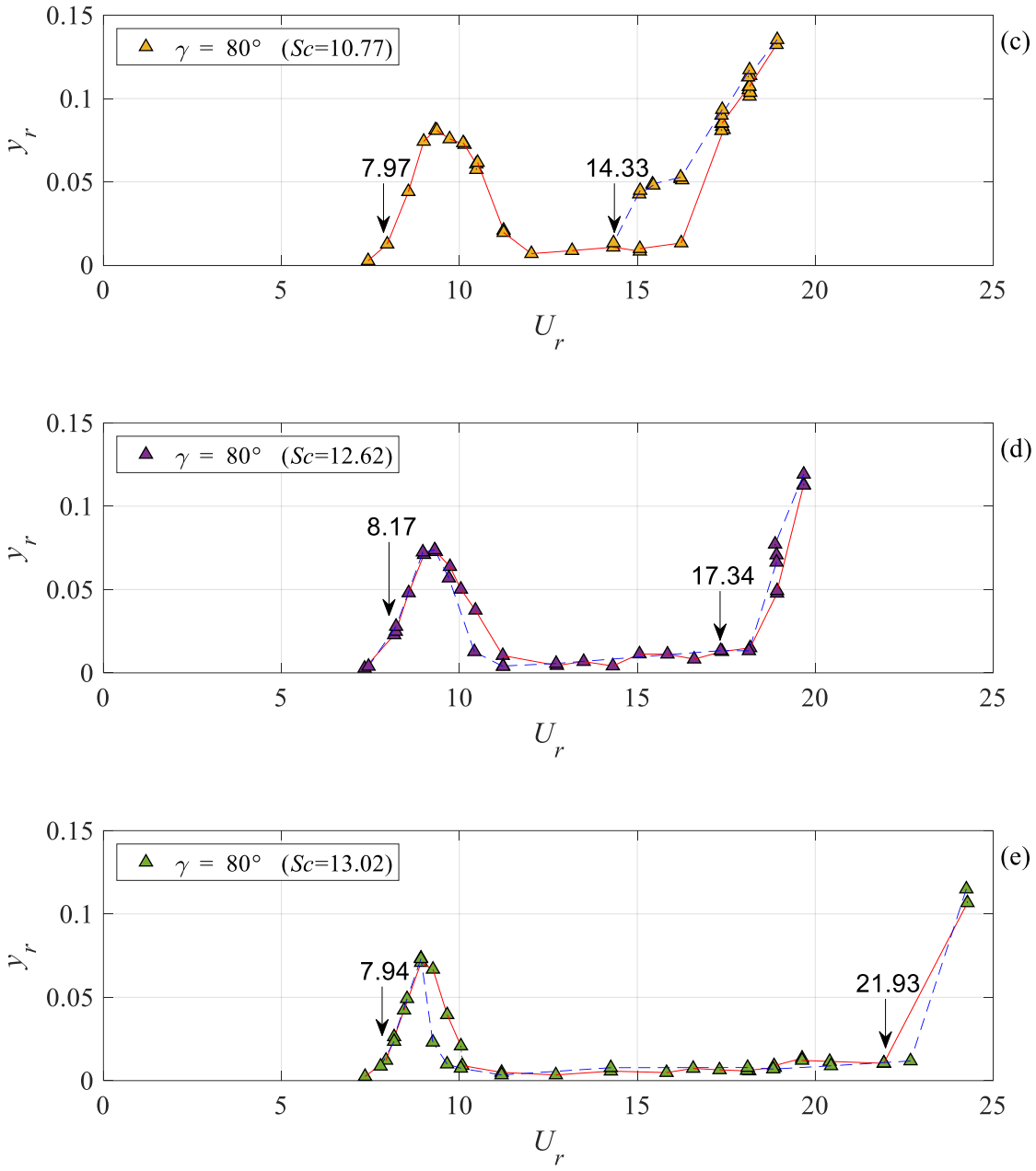

Fig. 8 Reduced amplitude versus reduced wind speed at angle of attack $\alpha = 10°$ for different orientations of the principal structural axes and different Scruton numbers: (a) Setup 1, $\gamma = 90°$ and $Sc = 23.66$; (b) Setup 2, $\gamma = 82°$ and $Sc = 13.11$; (c) Setup 3, $\gamma = 80°$ and $Sc = 10.77$; (d) Setup 4, $\gamma = 80°$ and $Sc = 12.62$; (e) Setup 5, $\gamma = 80°$ and $Sc = 13.02$; solid lines stand for increasing wind speed, dashed lines for decreasing wind speed

Table 2. Critical velocities for VIV and galloping from dynamic tests

Setup ID	γ	Sc	Reduced critical velocity for VIV $U_{V,r}$	Reduced critical velocity for galloping $U_{G,r}$	$U_{G,r}/U_{V,r}$
1	90°	23.66	7.56	14.97	1.98
2	82°	13.11	7.87	17.36	2.21
3	80°	10.77	7.97	14.33	1.79
4	80°	12.62	8.17	18.14	2.22
5	80°	13.02	7.94	21.93	2.76

4.2. Galloping responses

To have a further insight on the galloping responses of the square-section prism, the oscillation amplitudes for Setups 1, 2, 4 and 5 are re-plotted in Fig. 9, scaled with Sc and disregarding the VIV responses. The responses for Setup 3 are not plotted in Fig. 9 because separation between VIV and galloping is not as clear as in the other cases, as discussed in the previous section. The experimental results are also compared with the quasi-steady prediction. In this figure, for closed markers indicate increasing wind velocity while the open markers indicate decreasing velocity.

It can be seen from Fig. 9 that when the model is allowed to vibrate in the across-wind direction, i.e. the angle between wind direction and structural axis $\gamma = 90^o$, galloping occurs at the normalised wind speed $U_{cr,r}/Sc = 0.73$. This value is lower than that predicted by quasi-steady theory, which gives $U_{cr,r}/Sc = 1.06$. The unsuccessful prediction of the quasi-steady theory in this case agrees with the wind tunnel investigation by Carassale et al. [43], who stated that the theory fails to accurately predict the onset of galloping in the neighbour of the critical angle of attack, i.e. $\alpha=12^o$.

The prediction of the quasi-steady theory is improving for the non-across-wind galloping. For $\gamma = 82^o$ and Sc=13.11, galloping occurs at a normalised wind speed $U_{cr,r}/Sc$=1.32. The quasi-steady theory predicts that $U_{cr,r}/Sc = 1.51$, being an overestimate by 14%. For $\gamma = 80^o$, galloping occurs at a normalised wind speed $U_{cr,r}/Sc$=1.4 for Sc=12.62 and $U_{cr,r}/Sc = 1.7$ for Sc=13.62. In this case of γ, the quasi-steady theory predicts that $U_{cr,r}/Sc = 1.74$, being an overestimate by 24% and 2% for Sc=12.62 and Sc=13.62, respectively.

In summary, the observations confirm the theoretical prediction that the prism is more stable for the more inclination of the principal axis y to the wind, i.e. higher critical wind speed for smaller angle γ. The theory highly overestimates the critical wind speed for the occurrence of across-wind galloping. But it provides a relatively good estimate of the critical wind speed for the cases of non-across-wind galloping, with better prediction for higher Scruton number. It is worth remembering that the values derived from the quasi-steady theory are uncertain due to the uncertainty in evaluating the aerodynamic factors S_a. This affects the validation of the quasi-steady theory.

Finally, it is interesting to discuss the hysteresis phenomenon. To the authors' knowledge, only a few wind tunnel experimental studies have been conducted to study galloping hysteresis of square-section cylinders. The foundation work by Parkinson and Smith [5] and the recent work by Freda et al. [1] should be referred to this issue. Those experiments were conducted only for zero angle of attack and for across-wind galloping. The present study used an angle of attack of 10^o and tested for both across-wind and non-across-wind galloping ($\gamma = 80^o$, $\gamma = 82^o$ and $\gamma = 90^o$). It can be observed from Fig. 9 that, for across-wind galloping ($\gamma = 90^o$), there is no clear hysteresis region. This is in contrast to the experimental results from Parkinson and Smith [5], the theoretical investigation by Novak [6] and numerical simulations by Luo et al. [35], in which galloping hysteresis was always present and depended only on the aerodynamic coefficients. However, it agrees with the results from [1], in which the hysteresis was not always found, depending on Scruton number Sc. For the cases of non-across-wind galloping, hysteresis zones are more evident and are larger for higher Sc and the principal axis more inclined to the wind. Especially, for γ=80^o, the two hysteresis zones for the two value of Sc are separate instead of collapsed onto a single curve. The results show that the hysteresis depends also on structural parameter through Sc. The differences in behaviour identified here require further experimental and theoretical work to further understand the phenomenon.

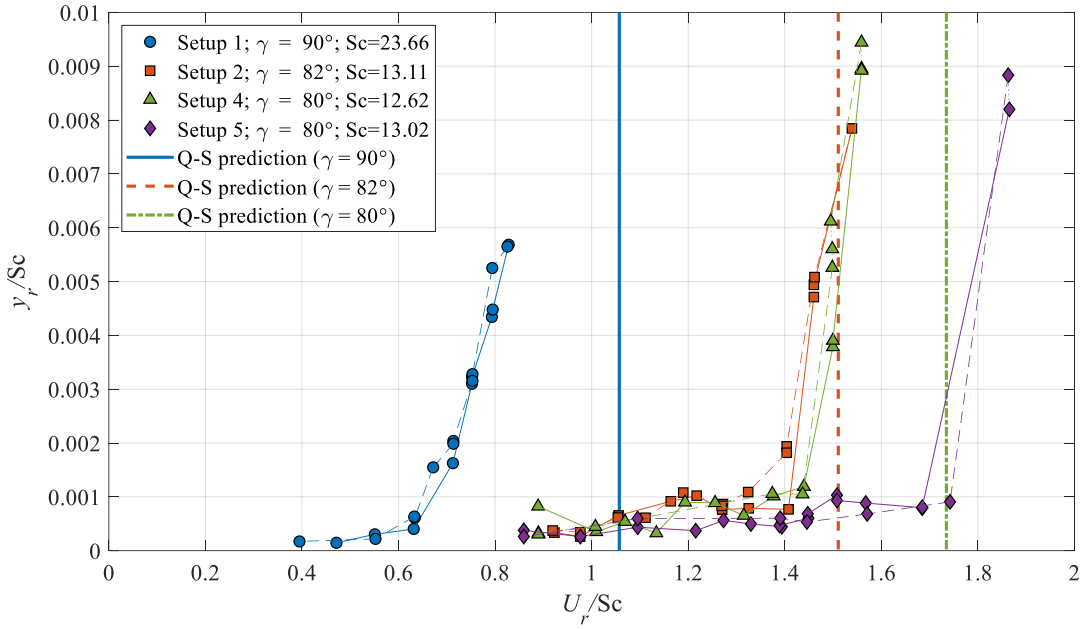

Fig. 9 Normalized galloping amplitudes for angle of attack $\alpha = 10°$ for different orientations of the principal structural axes, $\gamma = 80°$, 82° and 90°; solid lines stand for increasing wind speed, dashed lines for decreasing wind speed

5. Conclusions

The research on 1DOF galloping of prismatic cylinders is very rich in the literature, but only across-wind oscillations have previously been considered experimentally. The role of the orientation of the principal axes for the aeroelastic response of structures has never been addressed in wind tunnel tests. Understanding the onset and post-critical galloping behaviour when neither of the structural principal axes is normal to the wind is therefore of interest. Furthermore, most of the previous wind tunnel investigations on square prisms have been conducted for zero angle of attack. It is therefore necessary to increase understanding of galloping responses for other angles.

Focusing on a square sectional cylinder, this paper addresses non-across-wind galloping through new wind tunnel tests. By restricting the prism to vibrate in planes normal to or inclined to the wind direction, conventional across-wind galloping and non-across-wind galloping behaviour have been investigated. Various conclusions are drawn as follows:

- The theoretical and experimental results show that for a given angle of attack, the structure has different aeroelastic behaviour for different orientations of the structural axis.
- At an angle of attack of 10°, which is close to the critical angle of attack of square prisms,

quasi-steady theory is not successful in accurately predicting the critical wind velocity for the onset of across-wind galloping. However, the theoretical prediction agrees better with the experimental results for oscillations at 80° and 82° to the wind direction.

- There is clear separation between galloping and VIV when Sc is higher than 12 or the ratio between the onset critical wind speeds of galloping and VIV is higher than 2.

- The normalised onset and post-critical galloping responses are strongly dependet on the angle between the wind and the structural axis as well as on the Scruton number.

Although this paper focuses on galloping, VIV responses are also presented. The critical VIV wind speeds are close to the theoretical predicted value but are not identical for a given angle of attack but different Scruton numbers and structural axis directions. It is highlighted that further investigations on VIV behaviour of square prims for across-wind and non-across-wind vibrations and with different Scruton numbers and angles of attack. This is particularly important for prismatic cylinders with square sections due to the fact that there have been a few studies on VIV and VIV-galloping interaction compared with other sectional shapes, e.g. circular and rectangular sections.

6. Conflict of interest

The authors declare that there is no conflict of interest.

7. Acknowledgements

This research is funded by the Vietnam National Foundation for Science and Technology Development (NAFOSTED) under grant number 107.04-2017.321.

The authors would like to thank BMT Fluid Mechanics Ltd. for the use of their wind tunnel and their support and assistance during the testing campaign.

Finally, the authors gratefully acknowledge the Royal Academy of Engineering Newton Research Collaboration Programme, grant number NRCP/1415/292, for supporting the visit of the first author to the University of Bristol.

8. References

1. Freda A, Carassale L, Piccardo G (2015) Aeroelastic crosswind response of sharp-edge square sections : experiments versus theory. In: Proceedings of the 14th International Conference on Wind Engineering, Porto Alegre, Brazil – June 21-26, 2015
2. Ma CM, Liu YZ, Li QS, Liao HL (2018) Prediction and explanation of the aeroelastic behavior of a square-section cylinder via forced vibration. Journal of Wind Engineering and Industrial Aerodynamics 176:78–86.
3. Scruton C (1960) Use of wind tunnels in industrial aerodynamic research. AGARD Report 309, NPL Report 411
4. Parkinson G., Brooks PNH (1961) On the aeroelastic instability of bluff cylinders. Journal of Applied Mechanics 28:252–258
5. Parkinson G., Smith J. (1964) The square prism as an aeroelastic non-linear oscillator. Q J Mech Appl Math 17:225–239
6. Novak M (1969) Aeroelastic galloping of prismatic bodies. J Eng Mech Div -ASCE 96:115–142
7. Slater JE (1969) Aeroelastic instability of a structural angle section. University of British Columbia, Vancouver, B.C., Canada
8. Novak M (1972) Galloping oscillations of prismatic structures. J Eng Mech Div -ASCE 98:27–46
9. Kluger JM, Moon FC, Rand RH (2013) Shape optimization of a blunt body Vibro-wind galloping oscillator. Journal of Fluids and Structures 40:185–200.
10. Nguyen CH, Freda A, Solari G, Federica T (2015) Experimental investigation of the aeroelastic behavior of a complex prismatic element. Wind and Structures, An International Journal 20:683–699
11. Blevins RD (2001) Flow-induced Vibration, Second. Krieger Publishing company, Florida
12. Paidoussis M, Price S, De Langre E (2011) Fluid-Structure Interactions: cross-flow-induced instabilities. Cambridge University Press
13. Piccardo G, Pagnini LC, Tubino F (2014) Some research perspectives in galloping phenomena: critical conditions and post-critical behavior. Continuum Mechanics and Thermodynamics 27:261–285.
14. Nikitas N, Macdonald JHG (2014) Misconceptions and generalisations of the Den Hartog

galloping criterion. Journal of Engineering Mechanics, ASCE 140:1–11.

15. Nguyen CH (2013) Aerodynamic and Aeroelastic Analysis of Complex Structures. PhD thesis, University of Genoa

16. Hémon P, Amandolese X, Andrianne T (2017) Energy harvesting from galloping of prisms: A wind tunnel experiment. Journal of Fluids and Structures 70:390–402.

17. Hemon P (2012) Large Galloping Oscillations af a Square Section Cylindwer in Wind Tunnel. In: Proceeding of the 10th conference on Flow Induced Vibrations, FIV , Dublin, Ireland, July 3–6.

18. Kawai H (1995) Effects of angle of attack on vortex induced vibration and galloping of tall buildings in smooth and turbulent boundary layer flows. Journal of Wind Engineering and Industrial Aerodynamics 54–55:125–132.

19. Ma CM, Liu YZ, Li QS, Liao HL (2018) Prediction and explanation of the aeroelastic behavior of a square-section cylinder via forced vibration. Journal of Wind Engineering and Industrial Aerodynamics 176:78–86.

20. Cheng S, Larose GL, Savage MG, et al (2008) Experimental study on the wind-induced vibration of a dry inclined cable-Part I: Phenomena. Journal of Wind Engineering and Industrial Aerodynamics 96:2231–2253.

21. Jakobsen JB, Andersen TL, Macdonald JHG, et al (2012) Wind-induced response and excitation characteristics of an inclined cable model in the critical Reynolds number range. Journal of Wind Engineering and Industrial Aerodynamics 110:100–112.

22. Matsumoto M, Shiraishi N, Kitazawa M, et al (1990) Aerodynamic behaviour of inclined circular cylinders-cable aerodynamics. Wind Engineering and Industrial Aerodynamics 33:63–72

23. Matteoni G, Georgakis CT (2015) Effects of surface roughness and cross-sectional distortion on the wind-induced response of bridge cables in dry conditions. Journal of Wind Engineering and Industrial Aerodynamics 136:89–100.

24. Carassale L, Freda A, Piccardo G (2005) Instability mechanisms of skewed circular cylinders. In: The Fourth European and African Conference on Wind Engineering (EACWE4), Prague, Czech, July 2005

25. Mannini C, Marra AM, Bartoli G (2015) Experimental investigation on VIV-galloping interaction of a rectangular 3:2 cylinder. Meccanica 50:841–853.

26. Mannini C, Massai T, Marra AM, Bartoli G (2015) Modelling the interaction of VIV and galloping for rectangular cylinders. In: Proceedings of the 14th International Conference on Wind Engineering, Porto Alegre, Brazil – June 21-26, 2015

27. Glauert BH (1919) The rotation of an aerofoil about a fixed axis. Report and memoranda, No. 595, British Advisory Committee for Aeronautics (ARC) 443–447

28. Den Hartog JP (1932) Transmission line vibration due to sleet. Transactions of the American Institute of Electrical Engineers 51:1074–1076

29. Nguyen CH, Freda A, Solari G, Tubino F (2015) Aeroelastic instability and wind-excited response of complex lighting poles and antenna masts. Engineering Structures 85:264–276.

30. Carassale L, Freda A, Marrè-Brunenghi M (2013) Effects of free-stream turbulence and corner shape on the galloping instability of square cylinders. Journal of Wind Engineering and Industrial Aerodynamics 123:274–280.

31. Vinuesa R, Schlatter P, Malm J, et al (2015) Direct numerical simulation of the flow around a wall-mounted square cylinder under various inflow conditions. Journal of Turbulence 16:555–587

32. Lee BE (1975) The effect of turbulence on the surface pressure field of a square prism. Journal of Fluid Mechanics 69:263–282

33. Carassale L, Freda A, Marrè-Brunenghi M, et al (2012) Experimental investigation on the aerodynamic behavior of square cylinders with rounded corners. In: The Seventh International Colloquium on Bluff Body Aerodynamics and Applications (BBAA7), Shanghai, China; September 2-6, 2012. Shanghai, China

34. Tamura T, Miyagi T (1999) The effect of turbulence on aerodynamic forces on a square cylinder with various corner shapes. Journal of Wind Engineering and Industrial Aerodynamics 83:135–145.

35. Luo SC, Chew YT, Ng YT (2003) Hysteresis phenomenon in the galloping oscillation of a square cylinder. Journal of Fluids and Structures 18:103–118.

36. Barrero-Gil A, Sanz-Andrés A, Alonso G (2009) Hysteresis in transverse galloping: The role of the inflection points. Journal of Fluids and Structures 25:1007–1020.

37. Pagnini LC, Freda A, Piccardo G (2015) Uncertainties in the evaluation of one degree-of-freedom galloping onset. In: 14th International Conference on Wind Engineering – Porto

Alegre, Brazil – June 21-26, 2015. Porto Alegre, Brazil

38. Amandolèse X, Hémon P (2010) Vortex-induced vibration of a square cylinder in wind tunnel. Comptes Rendus - Mecanique 338:12–17.

39. Norberg C (1993) Flow around rectangular cylinders: Pressure forces and wake frequencies. Journal of Wind Engineering and Industrial Aerodynamics 49:187–196.

40. Nakamura Y, Mizota T (1975) Unsteady lifts and wakes of oscillating rectangular prisms. Journal of Engineering Mechanics 101:855–871

41. Parkinson G V., Wawzonek MA (1981) Some considerations of combined effects of galloping and vortex resonance. Journal of Wind Engineering and Industrial Aerodynamics 8:135–143.

42. EN 1991-1-4 (2005) Eurocode 1: Actions on structures -Part 1-4: General actions -Wind actions. European Committee for Standardization 4:1–148.

43. Carassale L, Freda A, Marrè-Brunenghi M (2014) Experimental investigation on the aerodynamic behavior of square cylinders with rounded corners. Journal of Fluids and Structures 44:195–204.